Available online at www.sciencedirect.com
ScienceDirect
Geochimica et Cosmochimica Acta 74 (2010) 4219–4233
Geochimica et Cosmochimica Acta
www.elsevier.com/locate/gca

High- and low-affinity binding sites for Cd on the bacterial cell walls of *Bacillus subtilis* and *Shewanella oneidensis*

Bhoopesh Mishra [a,*], Maxim Boyanov [c], Bruce A. Bunker [a], Shelly D. Kelly [c], Kenneth M. Kemner [c], Jeremy B. Fein [b]

[a] *Department of Physics, University of Notre Dame, Notre Dame, IN 46556, USA*
[b] *Department of Civil Engineering and Geological Sciences, University of Notre Dame, Notre Dame, IN 46556, USA*
[c] *Molecular Environmental Science Group, Biosciences Division, Argonne National Laboratory, Argonne, IL 60439, USA*

Received 31 August 2009; accepted in revised form 17 February 2010; available online 23 February 2010

Abstract

Bulk Cd adsorption isotherm experiments, thermodynamic equilibrium modeling, and Cd K edge EXAFS were used to constrain the mechanisms of proton and Cd adsorption to bacterial cells of the commonly occurring Gram-positive and Gram-negative bacteria, *Bacillus subtilis* and *Shewanella oneidensis*, respectively. Potentiometric titrations were used to characterize the functional group reactivity of the *S. oneidensis* cells, and we model the titration data using the same type of non-electrostatic surface complexation approach as was applied to titrations of *B. subtilis* suspensions by Fein et al. (2005). Similar to the results for *B. subtilis*, the *S. oneidensis* cells exhibit buffering behavior from approximately pH 3–9 that requires the presence of four distinct sites, with pK_a values of 3.3 ± 0.2, 4.8 ± 0.2, 6.7 ± 0.4, and 9.4 ± 0.5, and site concentrations of $8.9(\pm 2.6) \times 10^{-5}$, $1.3(\pm 0.2) \times 10^{-4}$, $5.9(\pm 3.3) \times 10^{-5}$, and $1.1(\pm 0.6) \times 10^{-4}$ moles/g bacteria (wet mass), respectively. The bulk Cd isotherm adsorption data for both species, conducted at pH 5.9 as a function of Cd concentration at a fixed biomass concentration, were best modeled by reactions with a Cd:site stoichiometry of 1:1. EXAFS data were collected for both bacterial species as a function of Cd concentration at pH 5.9 and 10 g/L bacteria. The EXAFS results show that the same types of binding sites are responsible for Cd sorption to both bacterial species at all Cd loadings tested (1–200 ppm). Carboxyl sites are responsible for the binding at intermediate Cd loadings. Phosphoryl ligands are more important than carboxyl ligands for Cd binding at high Cd loadings. For the lowest Cd loadings studied here, a sulfhydryl site was found to dominate the bound Cd budgets for both species, in addition to the carboxyl and phosphoryl sites that dominate the higher loadings. The EXAFS results suggest that both Gram-positive and Gram-negative bacterial cell walls have a low concentration of very high-affinity sulfhydryl sites which become masked by the more abundant carboxyl and phosphoryl sites at higher metal:bacteria ratios. This study demonstrates that metal loading plays a vital role in determining the important metal-binding reactions that occur on bacterial cell walls, and that high affinity, low-density sites can be revealed by spectroscopy of biomass samples. Such sites may control the fate and transport of metals in realistic geologic settings, where metal concentrations are low.

1. INTRODUCTION

Bacteria are ubiquitous in a wide range of low temperature aqueous systems, and aqueous metal adsorption onto bacterial cell wall functional groups can influence metal speciation, bioavailability, and transport (Ledin et al., 1996, 1999; Ledin, 2000; Ohnuki et al., 2007). Metal adsorption onto bacterial cell walls can be viewed as a surface complexation reaction, and the thermodynamic stabilities of a wide range of metal-bacterial surface complexes have been determined using bulk adsorption measurements (e.g., Fein et al., 1997; Small et al., 1999; Yee and Fein, 2001; Daughney et al., 2002; Yee and Fein, 2003; Borrok

* Corresponding author. Present address: Biosciences Division, Argonne National Laboratory, Argonne, IL 60439, USA.
E-mail address: bmishra@anl.gov (B. Mishra).

0016-7037/$ - see front matter © 2010 Elsevier Ltd. All rights reserved.
doi:10.1016/j.gca.2010.02.019

et al., 2004b; Wightman and Fein, 2005; Kulczycki et al., 2005; Burnett et al., 2006; Leone et al., 2007; Ngwenya, 2007; Pokrovsky et al., 2008a). In addition, X-ray absorption spectroscopy studies have identified cell wall carboxyl, phosphoryl, and sulfhydryl groups as important sites of metal binding (Hennig et al., 2001; Kelly et al., 2002; Panak et al., 2002; Boyanov et al., 2003; Toner et al., 2005; Guiné et al., 2006; Mishra et al., 2007; Pokrovsky et al., 2008b; Mishra et al., 2009). Most of these previous studies examined metal–bacterial adsorption under conditions with relatively high metal:bacterial site concentration ratios, and many of these studies focused on the pH dependence of adsorption rather than on the concentration dependence. While measurements of the pH dependence of metal adsorption onto bacteria place constraints on the cell wall sites responsible for the binding, measurements conducted as a function of metal:ligand ratio better constrain the metal:site stoichiometry of the adsorption reactions than do standard pH edge adsorption experiments. Furthermore, the important binding mechanisms can change as a function of metal:ligand concentration ratio, and studies at relatively high and fixed metal concentrations may mask the presence and importance of low concentration, high affinity metal binding sites on surfaces (Sarret et al., 1998).

Extended X-ray absorption fine structure (EXAFS) spectroscopy has demonstrated that only a limited number of binding sites are responsible for metal binding onto cell walls from a range of bacterial species. Phosphoryl and carboxyl functional groups are responsible for metal complexation by both Gram-positive bacteria (Kelly et al., 2002; Boyanov et al., 2003) and Gram-negative bacteria (Toner et al., 2005; Hennig et al., 2001; Panak et al., 2002) despite fundamental differences in molecular structure of their exterior surfaces. These two functional groups have also been found responsible for metal binding in both natural and contaminated consortia of bacteria obtained from river water and a manufactured gas plant site, respectively (Mishra et al., 2009). However a Cd-sulfhydryl binding site was also identified in the river water consortium (Mishra et al., 2009). Using infrared spectroscopy, Wei et al. (2004) studied both Gram-positive and Gram-negative bacterial surface functional groups and determined that phosphoryl and carboxyl groups are the primary contributors to the negative charge, and hence the reactivity of the bacterial cell wall.

Relatively few studies have investigated the mechanisms of metal complexation with bacterial cell walls as a function of metal loading. Sarret et al. (1998) examined Zn and Pb sorption to fungal cell walls of *Penicillium chrysogenum* at pH 6 as a function of Zn and Pb loading, and the phosphoryl group was found to be the predominant complexing ligand. Carboxyl binding was significant only under the highest Zn loading and the lowest Pb loading conditions. Burnett et al. (2006) studied Cd adsorption onto the thermophilic species *A. flavithermus*, and found that at high bacteria:Cd ratios Cd adsorption occurs by formation of a 1:1 complex with deprotonated cell wall carboxyl functional groups. At lower bacteria:Cd ratios, a second adsorption mechanism occurs at pH > 7, which may correspond to the formation of a Cd-phosphoryl, CdOH-carboxyl, or CdOH-phosphoryl surface complex. Guiné et al. (2006) reported the importance of sulfhydryl ligands in addition to phosphoryl and carboxyl ligands in the adsorption of Zn onto three Gram-negative bacterial strains (*Cupriavidus metallidurans* CH34, *Pseudomonas putida* ATCC12633, and *Escherichia coli* K12DH5α) at low loadings of Zn. Mishra et al. (2007) reported that sulfhydryl ligands, in addition to carboxyl and phosphoryl sites, were required for EXAFS modeling of Cd binding with the Gram-negative bacteria *Shewanella oneidensis* and an aquatic consortium of bacteria at 30 ppm Cd loading and 10 g/L (wet mass) biomass. However, sulfhydryl ligands were not required for EXAFS modeling of the Gram-positive bacteria *Bacillus subtilis* under the same conditions, consistent with previous finding by Boyanov et al. (2003). Similarly, Pokrovsky et al. (2008b) observed Cd complexation with sulfhydryl functional groups on the marine anoxygenic bacteria *R. palustris* in systems with 3 ppm Cd and 4 g/L biomass. While the Cd-sulfhydryl binding by Mishra et al. (2007) and Pokrovsky et al. (2008b) was observed in systems near pH 6, Mishra et al. (2009) demonstrated that aquatic consortia of bacteria exhibit sulfhydryl binding of Cd across a wide pH range and even at relatively elevated Cd concentrations.

The objective of this study is to explore metal–bacterial adsorption reactions using both bulk adsorption measurements and X-ray absorption spectroscopy over a wide range of metal:ligand ratios, and to compare these results for the Gram-positive bacterial species *B. subtilis* and the Gram-negative bacterial species *S. oneidensis*. Cell wall functional group reactivity for *B. subtilis* has been characterized by Fein et al. (2005), and we collect new potentiometric titration data in this study using *S. oneidensis* in order to determine the site concentrations and acidity constants for the important binding sites on the *S. oneidensis* cell wall. Thermodynamic equilibrium modeling of the bulk adsorption data was used to constrain the stoichiometries of the important proton and Cd adsorption reactions. EXAFS measurements were conducted at pH 5.9, over a wide range of Cd concentrations (1–200 ppm for *B. subtilis* and 3–200 ppm for *S. oneidensis*) at a fixed bacterial concentration of 10 g/L (wet mass), and we use these data to constrain the molecular-scale Cd adsorption mechanisms and to determine whether the adsorption mechanisms change as a function of Cd loading onto the bacterial cell walls.

Although Cd binding onto *B. subtilis* cells has already been studied using EXAFS by members of our group previously (Boyanov et al., 2003), the goals of this study are fundamentally different. While Boyanov et al. (2003) studied the adsorption behavior of *B. subtilis* over a pH range of 3.4–7.8 at a fixed Cd:biomass ratio, this study attempts to determine the site stoichiometry, and the sequence of reactions occurring on bacterial cell walls as a function of Cd loading at a fixed pH.

2. METHODS AND MATERIALS

2.1. Bacterial growth and harvest

S. oneidensis str., formerly classified as *S. putrefaciens* MR-1 (Venkateswaren et al., 1999), is a Gram-negative

dissimilatory metal-reducing bacterium found in soils, sediments, surface waters, and ground waters (e.g., Sorenson, 1982; Nealson and Myers, 1992). *B. subtilis* is an aerobic Gram-positive soil microorganism with well-characterized surface charge and reactivity (Harden and Harris, 1952; Beveridge and Murray, 1980; Fein et al., 1997,2005). The bacterial growth and wash procedures used in this study were identical for both bacterial species and similar to those described in Fein et al. (2005). A plated colony was transferred from an agar plate to a test tube containing 7 mL of sterilized trypticase soy broth (TSB) + 0.5% yeast extract. Each broth tube was then incubated for 24 h at 32 °C in an incubator/shaker. The subsequent bacterial suspension was then transferred to 1 L of TSB + 0.5% yeast extract and incubated for another 24 h at 32 °C in the incubator/shaker. The cells were removed from the nutrient medium by centrifugation and rinsed five times with 0.1 M $NaClO_4$ (the electrolyte used in the experiments). The cells were not acid washed in order to avoid disruption of the cell wall structure (Borrok et al., 2004a). Biomass is cited in terms of wet mass, determined by centrifugation at 5800*g* for 60 min, and corresponds to approximately eight times the dry mass of the cells (Borrok et al., 2005).

2.2. Potentiometric titrations

Three replicate potentiometric titrations were performed, each using 100 g/L (wet mass) suspensions of *S. oneidensis* in 0.1 M $NaClO_4$. The electrolyte solution was bubbled with N_2 gas for 1 h prior to use, and the titration cell containing the bacterial suspension was kept under a N_2 atmosphere during the experiment. The sample was continuously stirred with a small magnetic stir bar during the titration. The titrations were first run down-pH from an initial pH of approximately 4 with aliquots of 1.0005 *N* HCl to approximately pH 2.7, then up-pH with aliquots of 1.005 *N* NaOH to approximately pH 9.5. Each addition of acid or base occurred only after a stability of 0.01 °mV/s was attained. Although it is likely that the buffering capacity of the bacterial cell wall extended to extremely low pH conditions (e.g., Fein et al., 2005), we limited the potentiometric titrations to a low pH value of 2.7 in order to avoid excessive disruption of the Gram-negative cell wall structure (Borrok et al., 2004a).

2.3. Cd adsorption experiments

Washed bacteria were suspended in high density polyethylene test tubes containing 0.1 M $NaClO_4$ electrolyte to form a suspension of 10 g/L of bacteria (wet mass). A 500 ppm parent solution of Cd in 0.1 M $NaClO_4$ was prepared from a commercially-supplied 1000 ppm Cd reference solution. The pH of this parent solution was adjusted to 5.9 by adding small aliquots of 1 M NaOH. Appropriate amounts of the parent solution were added to the bacterial suspensions, and these suspensions were topped off with additional 0.1 M $NaClO_4$ to achieve the desired Cd and bacterial concentrations. The pH of each system was adjusted using small aliquots of 1 M HNO_3 or NaOH, and the systems were allowed to react for 2 h on a shaker. The concentrations of total Cd in the experimental systems ranged from 0.25 to 200 ppm. Previous studies involving *B. subtilis* have demonstrated that equilibrium of Cd adsorption reactions occurs in less than 1 h, and that the adsorption reactions are fully reversible (e.g., Fowle and Fein, 2000). pH was monitored every 30 min, and adjusted as required using minute aliquots of 1 M HNO_3 or NaOH. The final pH was measured after two hours, and the solution was then centrifuged. The final pH of each experimental system was 5.9 ± 0.1, and the pH of the solutions never varied by more than 0.3 during the course of the experiments. The bacterial pellet was retained for X-ray absorption spectroscopy analysis, and the resultant supernatant was filtered (0.45 μm) and analyzed for dissolved Cd using an inductively coupled plasma-optical emission spectroscopy technique with matrix-matched standards. The concentration of metal adsorbed to bacteria in each vessel was calculated by subtracting the concentration of metal that remained in solution from the original Cd concentration in the experiment.

2.4. EXAFS measurements and data reduction

EXAFS is a powerful structural probe that provides information on the short-range coordination environment of the atom under study (Stern, 1974). Fluorescence mode Cd K edge (26,711 eV) EXAFS measurements were performed at MRCAT, sector 10-ID beamline of the Advanced Photon Source at Argonne National Laboratory (Segre et al., 2000). The energy of the incident X-rays was scanned by using a Si(1 1 1) reflection plane of a cryogenically-cooled double-crystal monochromator. The third harmonic of the undulator was utilized, with an undulator tapering of about 3.5 keV to reduce the variation in the incident intensity to less than 15% over the scanned energy range. X-rays of higher harmonic energies were removed using grazing incidence reflection from a Pt-coated mirror. The incident ionization chamber was filled with 100% N_2 gas. The transmitted and reference ion chambers were filled with 100% Ar gas. The fluorescence detector in the Stern–Heald geometry (Stern and Heald, 1983) was filled with Kr gas, and a Pd filter of six absorption lengths was used to reduce the background signal. The incident X-ray beam profile was 1 mm square. Linearity tests (Kemner et al., 1994) indicated less than 0.1% nonlinearity for a 50% decrease in incident X-ray intensity. Several energy scans were collected from each sample. All scans were aligned by using the simultaneously collected absorption spectrum of a Cd foil, by setting the first inflection point of the spectrum at 26,711 eV.

The homogeneous bacterial pellet that formed at the base of each experimental test tube was loaded into a slotted Plexiglas holder, covered with Kapton film, and transported immediately to the beamline for EXAFS measurements. All the EXAFS measurements were performed within 30 h of the adsorption experiment, and the samples were refrigerated during the entire time between adsorption experiment and EXAFS measurements. Quick scans (continuous-scanning mode of the monochromator), with signal sampling every 0.5 eV and an integration time of 0.1 s per

point were used. The advantage of using quick-scans is that it reduces the radiation exposure during a single scan. Consecutive spectra were monitored for possible radiation-induced changes; no changes were observed. To further reduce the possibility of radiation-induced changes or of sample inhomogeneity, the X-ray beam was moved to a fresh spot every 5 scans. A total of 30–150 consecutive scans from each sample were collected and averaged, depending on the Cd concentration in the sample.

Data were analyzed using the UWXAFS package (Stern et al., 1995). Processing of the raw data, including alignment of datasets and background removal, were implemented by using ATHENA (Ravel and Newville, 2005), IFEFFIT (Newville, 2001) and AUTOBK (Newville et al., 1993). The input parameter to ATHENA that determines the maximum frequency of the background, R_{bkg}, was set to 1.1 Å (Newville et al., 1993). The data range used for Fourier transforming the EXAFS $\chi(k)$ data was 2.3–9.8 $Å^{-1}$ with a Hanning window function and a dk value of 1.0 $Å^{-1}$ (Newville et al., 1993). Simultaneous fitting of each dataset with multiple k-weighting (k^1, k^2, k^3) of each spectrum was performed using the Fourier transformed $\chi(R)$ spectra. The fitting range for all of the datasets was 1.2–3.4 Å. The simultaneous fitting approach reduces the possibility of obtaining erroneous parameters due to correlations at any single k-weighting (Kelly et al., 2002; Mishra et al., 2009).

2.5. EXAFS standards

Powder and aqueous Cd standards were used to determine the spectral features of Cd in carboxyl, phosphoryl and sulfhydryl binding environments. A CdS powder standard was prepared from commercially available chemicals (Sigma–Aldrich), after grinding and sieving (~400 mesh). The aqueous Cd standards included Cd-acetate, and Cd-phosphate solutions. All aqueous Cd standards were prepared by dissolving $Cd(NO_3)_2.4H_2O$ in the appropriate acid/electrolyte. The Cd-acetate and Cd-phosphate standards were prepared with a Cd:ligand ratio of 1:100 (acetate or phosphate), by adding appropriate amounts of acetic and phosphoric acids. The pH of the Cd-acetate solution was adjusted using NaOH to 4.5, where the aqueous Cd-acetate aqueous complexes dominate the Cd speciation in solution. The pH of the Cd-phosphate solution was kept at 3.0 to avoid precipitation of a cadmium phosphate solid phase. Although the choice of standards is of paramount importance when applying a linear combination fitting approach to X-ray absorption near edge structure (XANES) data, EXAFS analysis is model independent. The main use of experimental standards is to fine-tune the fitting parameters for a given signal against a theoretical EXAFS signal generated by simulating a known crystal structure (as explained below). Therefore, the choice of aqueous versus crystalline standards for EXAFS analyses is not critical, and the use of a crystalline CdS powder as a standard for the biomass Cd–S EXAFS signal, when all other standards are aqueous, is acceptable.

EXAFS data analysis is based on refining theoretical EXAFS spectra against the experimental data. Models are constrained by use of crystalline model compounds with well-characterized local structures. The crystallographic information of the standard compounds were first transformed into a cluster of atoms by using the program ATOMS (Ravel, 2001). Then FEFF8 (Ankudinov et al., 1998) was used to carry out self-consistent quantum mechanical calculations to simulate theoretical EXAFS spectra based on the cluster of atoms thus obtained. Experimentally obtained EXAFS data on the standard compounds were fit to these theoretically generated EXAFS spectra using the program FEFFIT (Newville et al., 1995). We refined *ab initio* calculations on clusters of atoms derived from known crystal structures (Caminiti, 1982; Caminiti et al., 1984) against the EXAFS data from powdered CdS and aqueous Cd-acetate and Cd-phosphate standards.

The value obtained for the EXAFS amplitude reduction factor for all standards was $S_0^2 = 1.00 \pm 0.03$, and this value was used in modeling the spectra from the bacterial samples. Statistically significantly lower R factor and χ_v^2 values were used as criteria for improvement in the fit to justify the addition of an atomic shell to the model (Kelly et al., 2002).

3. RESULTS AND DISCUSSION

3.1. Potentiometric titrations

The three replicate titration curves are similar and are depicted in Fig. 1 as the mass normalized net molality of H^+ added versus pH. The mass normalized net molality of H^+ added is equal to the concentration of acid added to the system minus the concentration of base added, divided by the mass of the bacteria (in g/L; wet mass) used in the titration. Similar to other bacterial titrations (e.g., Plette et al., 1995; Fein et al., 1997; Daughney et al., 1998; Cox et al., 1999; Yee and Fein, 2003; Yee et al., 2004; Haas et al., 2001; Sokolov et al., 2001; Martinez et al., 2002; Ngwenya et al., 2003; Smith and Ferris, 2003; Claessens et al., 2004; Fein et al., 2005), our potentiometric titration data indicate that *S. oneidensis* exhibits significant proton buffering over the entire pH range studied. This finding indicates that the bacterial cell wall was not fully protonated, even under the lowest pH conditions attained (~2.7), and it is possible that proton-active functional groups are important contributors to the buffering at even lower pH values. The potentiometric titration data obtained by Haas et al. (2001), Sokolov et al. (2001), and Smith and Ferris (2003) for *S. putrefaciens* exhibit positive values for the mass normalized net molality of H^+ added to solution below pH values of approximately 7, with negative values at higher pH. Similar to those previous studies, the mass normalized net molality of H^+ added in this study is positive below a pH of approximately 7.5–8.0, and exhibits negative values at higher pH conditions. Although some previous studies have done so, the sign of this parameter should not be interpreted to indicate the sign of the surface charge of the bacterial surface at a particular pH value. Rather, the excess or deficit of this parameter relative to its value for a bacteria-free blank at the same pH indicates only that protons have been taken up or released by the

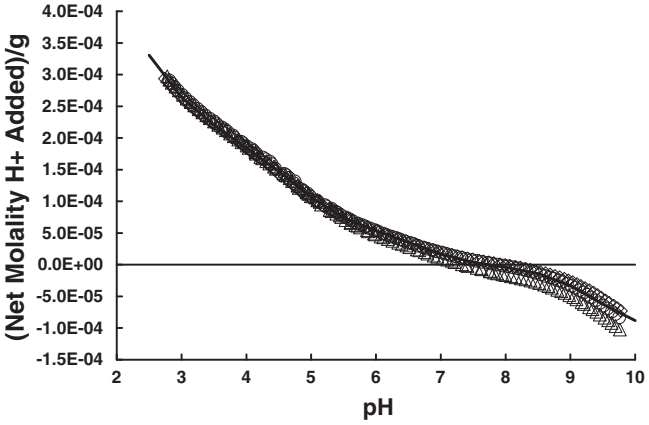

Fig. 1. Three replicate titration curves of *S. oneidensis* (50 g/L, wet wt.) in 0.1 M $NaClO_4$. Open diamonds, circles, and triangles represent experimental data points for individual titrations. Solid curve represents the average model fit.

bacteria. Electrophoretic mobility measurements indicate an overall negative charge associated with the *S. oneidensis* cell wall (Claessens et al., 2004). Therefore, we model the charging behavior of *S. oneidensis* with a series of organic acid functional group sites. We use a surface complexation approach to model the potentiometric titration and Cd adsorption data in order to relate pH and sorbent:sorbate ratio effects on adsorption to the speciation of the bacterial surface. Our first step is to model the potentiometric titration data to determine site concentrations and stability constants for the important surface reactive sites. A generalized deprotonation reaction for bacterial surface sites is represented as:

$$R - A_i H^\circ = R - A_i^- + H^+ \quad (1)$$

where R–A_i represents a bacterial surface functional group type and i is an integer $\geqslant 1$. A generalized mass action equation for the above reaction is:

$$Ka_{(i)} = \frac{[R - A_i^-]a_{H^+}}{[R - A_i H^0]} \quad (2)$$

where Ka and a represent the equilibrium (acidity) constant and activity of the subscripted reaction or species, respectively, and the brackets represent the concentration of surface sites in moles/L of solution. Each bacterial site R–A_i represents a discrete site with its own site concentration and acidity constant. FITEQL (Westall, 1982) was used as the computational tool to determine the number of discrete sites necessary to account for the observed buffering behavior and to solve for the site concentrations and acidity constants for each type of site. We used a non-electrostatic surface complexation model to describe proton and Cd adsorption onto the bacterial cell wall functional groups (e.g., Fein et al., 2005).

For each model tested, FITEQL calculates a variance function, V(Y), that describes the goodness-of-fit of the model to the experimental measurements. The best-fitting model was determined to be the one that yields the lowest V(Y) value to the experimental data. Each titration was modeled separately. A 4-site model with four deprotonation reactions associated with each site provides the best fit to the experimental data of all three bacterial titrations, with an average $V(Y) = 0.52$. Models utilizing less than 4-sites yield significantly higher V(Y) values and exhibit a worse visual fit to the experimental data. Models utilizing more than 4-sites fail to converge, indicating that the experimental data do not support more than four discrete sites. The average model fit to all three bacterial titrations is illustrated as a solid curve in Fig. 1. The best-fitting reaction stoichiometries with corresponding averaged deprotonation constants and averaged site concentrations for the *S. oneidensis* bacterial surface are given in Table 1.

Borrok et al. (2005) reviewed and compiled the available potentiometric titration datasets for individual bacterial species, bacterial consortia, and bacterial cell wall components, and derived an internally consistent thermodynamic model, similar to the model used in this study, for all the datasets. Borrok et al. (2005) found that, if one assumed a 4-site model for each titration dataset with pK_a values fixed to 3.1, 4.7, 6.6, and 9.0, the calculated site concentrations for the individual datasets were remarkably similar, yielding best-fit values of 1.13×10^{-4}, 9.08×10^{-5}, 5.32×10^{-5}, and 6.63×10^{-5} moles/g bacteria (wet mass) for the site concentrations for the lowest to the highest pK_a sites, respectively. The site concentrations and deprotonation constants that we determined for *S. oneidensis* (Table 1) are within uncertainties of the averages obtained by Borrok et al. (2005).

3.2. Cd adsorption

The results of the bulk adsorption measurements for *B. subtilis* and *S. oneidensis* are shown in Fig. 2a and b, respectively. The observed extents of Cd adsorption for the two

Table 1
Log K and site concentration values of *S. oneidensis* surface sites.

[Site][a]	Reaction	Log K
$8.9\ (\pm 2.6) \times 10^{-5}$	$R\text{–}A_{(1)}H^0 \leftrightarrows R\text{–}A_{(1)}^- + H^+$	-3.3 ± 0.2
$1.3\ (\pm 0.2) \times 10^{-4}$	$R\text{–}A_{(2)}H^0 \leftrightarrows R\text{–}A_{(2)}^- + H^+$	-4.8 ± 0.2
$5.9\ (\pm 3.3) \times 10^{-5}$	$R\text{–}A_{(3)}H^0 \leftrightarrows R\text{–}A_{(3)}^- + H^+$	-6.7 ± 0.4
$1.1\ (\pm 0.6) \times 10^{-4}$	$R\text{–}A_{(4)}H^0 \leftrightarrows R\text{–}A_{(4)}^- + H^+$	-9.4 ± 0.5

[a] Site concentrations in moles/g.

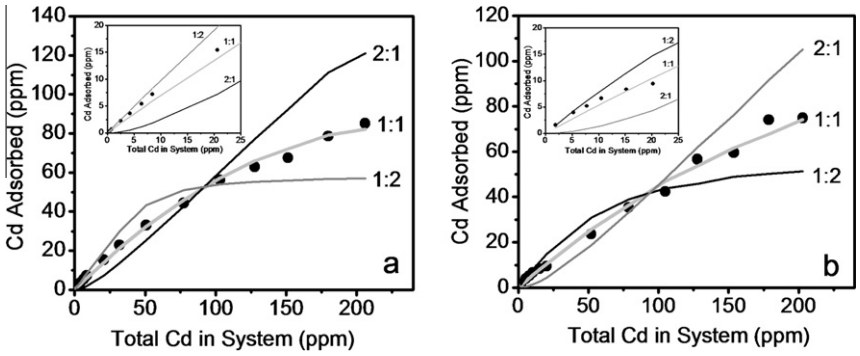

Fig. 2. Experimental data and models for different Cd:Site stoichiometries for (a) *B. subtilis,* and (b) *S. oneidensis.* These experiments were conducted at pH 5.9 ± 0.2, and the 10 g/L bacterial solution was prepared in a 0.1 M $NaClO_4$ electrolyte. The low Cd concentration range of the experimental data has been expanded for clarity and shown as insets in Figs. 2a and b.

bacterial species are similar. For each species, the concentration of adsorbed Cd increases with increasing total Cd in the experimental systems, but the slope decreases at higher Cd concentrations. Under the lowest Cd concentrations studied, Cd is predominantly adsorbed to the solid phase, while at higher total Cd concentrations a higher proportion remains in solution. Such adsorption behavior is typical for a system with a limited number of binding sites, in which sites are undersaturated at low metal concentrations and become increasingly saturated with increasing metal loading.

3.3. Thermodynamic modeling of the adsorption isotherms

Adsorption experiments that are conducted as a function of solute:sorbent concentration ratio at a fixed pH do not uniquely define which sorbing site or sites of a multi-site sorbent are responsible for the uptake, but the results do place rigorous constraints on the average stoichiometry of the adsorption reactions. A generic Cd adsorption reaction can be represented as an interaction between the aqueous Cd cation (Cd^{+2}) and deprotonated surface sites on the bacterial cell wall to create a bacterial surface complex:

$$x(Cd^{+2}) + y(R - A_i^{-1}) \Longleftrightarrow (R - A_i)_y(Cd)_x^{(2x-y)+} \quad (3)$$

where x and y represent stoichiometric coefficients that must be determined experimentally. We use the discrete 4-site non-electrostatic model of Fein et al. (2005) to describe the protonation state of the cell wall functional groups for *B. subtilis;* and we use the similar model for *S. oneidensis* from this study. The pK_a values for the four sites on *B. subtilis* are 3.3, 4.8, 6.8, and 9.1, respectively, and the corresponding site concentrations are 8.1×10^{-5}, 1.1×10^{-4}, 4.4×10^{-5}, and 7.4×10^{-5} moles of sites/gm wet mass bacteria, respectively (Fein et al., 2005). We refer to these sites as Sites 1–4, respectively.

Because the adsorption experiments were conducted under fixed pH conditions, the data can be equally well modeled by ascribing Cd adsorption onto any of the four site types on the bacterial cell wall, and more than one site may be involved in Cd binding under the experimental conditions. However, because the experiments were conducted at pH 5.9, we choose to model the Cd adsorption data for each bacterial species as an interaction between Cd^{2+} and the deprotonated form of Site 2 (the site with a pK_a value of 4.8 for both *B. subtilis*, and *S. oneidensis*). This exercise is intended only to constrain the average site stoichiometry of the important Cd–bacterial complexes at pH 5.9, and does not provide a molecular-scale understanding of the Cd binding environment. We attempted to model the Cd adsorption data using Cd:Site stoichiometries of 1:1, 1:2 and 2:1, using the V(Y) fit parameter from FITEQL to distinguish the best-fitting stoichiometry. The value of V(Y) depends on estimates for standard deviation in the experimental data, but in general V(Y) values between 0.1 and 20 represent reasonable fits, and models with lower V(Y) values represent better fits of the model to the data (Westall, 1982). Even if the reaction mechanism changes as a function of Cd loading, that is if different binding sites are important under different Cd loading conditions, this approach determines the average reaction stoichiometry for each binding mechanism.

The best-fitting models for each reaction stoichiometry are shown in Fig. 2a and b. The low Cd concentration range of the experimental data has been expanded for clarity and shown as insets in Fig. 2a and b. The V(Y) values associated with the best-fitting 1:1, 1:2, and 2:1 Cd:Site stoichiometry models for *B. subtilis* are 10.6, 320.1, and 174.9, respectively, indicating that the 1:1 model yields the best overall fit to the experimental data over the entire Cd concentration range. Fig. 2a illustrates that the 1:1 model fit to the data, with a calculated best-fit log K value for reaction (3) of 3.4 ± 0.2, provides a better fit than do the 1:2 or the 2:1 models when considering the entire Cd concentration range. The inset figure shows that the data cannot distinguish between the 1:1 and the 1:2 models under low Cd concentration conditions, so under these conditions, as the Cd concentration decreases and as the site:Cd molal ratio increases, it is possible that a surface complex with a 1:2 Cd:site stoichiometry becomes important. Similarly for *S. oneidensis*, the V(Y) values associated with the best-fitting 1:1, 1:2, and 2:1 Cd:Site stoichiometry models over the entire Cd concentration range studied are 20.9, 238.3, and 351.5, respectively. Fig. 2b demonstrates that the 1:1 model fit to the *S. oneidensis* data, also with a calculated best-fit

log K value for reaction (3) of 3.4 ± 0.3, provides a good fit to the experimental Cd adsorption data over the entire range of Cd concentrations. As is the case for the *B. subtilis* data in Fig. 2a, the data cannot distinguish between the 1:1 and the 1:2 models under low Cd concentration conditions, so it is possible that under these conditions a surface complex with a 1:2 Cd:site stoichiometry becomes important. It should be noted that Cd may be bound to more than one site under the experimental conditions, so the best-fit log K values reported here represent averages of the stability constant values for all of the important Cd–bacterial surface complexes.

The modeling results for *B. subtilis* and *S. oneidensis* are remarkably similar. The two bacterial species exhibit similar extents of adsorption over the entire range of Cd concentrations studied, and because of their similar proton reactivities and site concentrations, the calculated log K values for reaction (3) are within error of each other. Although these data do not constrain which site is involved in Cd binding, the 1:1 model yields the best fit to the entire Cd concentration range dataset regardless of which site we use in the model. If more than one site is involved in the Cd binding over this range of Cd loadings, the modeling suggests that any mechanism involves a 1:1 metal:site binding ratio, except perhaps under the lowest Cd concentration conditions studied here where a 1:2 complex is also possible.

3.4. Analysis of XAFS data from standard compounds

The fitting results for the Cd standards are shown in Table 2. The coordination environment of Cd in the acetate-bearing standard was modeled with O and C shells, corresponding to a bound acetate group. Data were fit with 5.5 (±0.3) O atoms in the first shell and 3C (fixed to this value based on speciation calculation) atoms in the second shell, consistent with the bidentate bonding mechanism observed by CaminitI et al. (1984). The Cd–C distance in the Cd-acetate standard was found to be 2.70 (±0.02) Å. The aqueous Cd-phosphate standard data were fit with 5.8 (±0.3) O atoms in the first shell, and 1.5 (±0.3) P atoms in the second shell. The Cd–O bond length was found to be 2.28 (±0.02) Å, the same distance as in the Cd-acetate standard, and the Cd–P bond distance was found to be 3.41 (±0.03) Å. The Cd sulfide standard was fit with 4 S atoms in the first shell at a distance of 2.53 (±0.02) Å. The sulfide standard displays characteristic spectral features that can be seen in Fig. 3a. The second and third oscillations of the Cd sulfide spectrum are out of phase relative to all the other standards. The phase shift arises from Cd bonding to sulfur in the first shell, as opposed to bonding to oxygen in all of the other standards. This phase shift (and change in frequency) in the chi data is manifested in a shift in the first peak of the Fourier transformed data for the Cd–S spectrum in Fig. 4a relative to the other standard spectra. In the Cd-acetate data, note the reduction in amplitude of the first shell peak in Cd-acetate compared to the Cd-phosphate spectrum (Fig. 4a). Detailed modeling reveals that the reduction in amplitude is due to the signal from the carbon atom interfering destructively with that from the oxygen atom. The subtle features in the second shell of the Cd-phosphate and Cd-acetate spectra are not seen clearly from the full view of the magnitude of the Fourier transformed data, because C and P are both light elements that do not backscatter the photoelectrons strongly. The enlarged real part of the Fourier transformed data, however, illustrates the relatively small changes in the second shell of the Cd-acetate and Cd-phosphate spectra (Fig. 4b). As can be seen from Fig. 4b, the Cd-phosphate standard exhibits a feature (line shape) at about 2.7 Å, indicative of the P atom in a bound phosphate group. The position of the S peak overlaps the position of the C feature at 2.2 Å in the Cd-acetate spectrum, but is shifted to larger distances. From the above analysis it is clear that the characteristic spectral features of a Cd-carboxyl and a Cd-phosphoryl local environment are: (1) for Cd-carboxyl binding, a smaller first shell peak amplitude exists, associated with an increase in the second shell peak at about 2.2 Å (Fig. 4b), and (2) for Cd-phosphoryl binding, a larger first shell amplitude is evident, along with a feature at 2.7 Å. The characteristic feature of Cd-sulfhydryl binding is a shifted first shell peak to larger distances relative to a Cd–O environment, and this shift is associated with an increase in the peak to a position just over 2.2 Å (Fig. 4b).

Table 2
Structural parameters obtained from fits of the standard compounds spectra.

Standard	Path	N	R(Å)	σ^2 (10^{-3} Å^2)
CdAc	Cd–O	5.5 ± 0.3	2.28 ± 0.02	10.9 ± 0.9
	Cd–C	3.0[b]	2.70 ± 0.02	12.8 ± 4.0
$CdPO_4$	Cd–O	5.8 ± 0.3	2.28 ± 0.02	10.5 ± 1.2
	Cd–P	1.5 ± 0.3	3.41 ± 0.03	15.0 ± 3.0
CdS	Cd–S	4.0[a]	2.53 ± 0.02	9.0 ± 1.0
	Cd–Cd	12.0[a]	4.2 ± 0.01	25.0 ± 4.0

[a] Fixed to this value based on crystallographic data.
[b] Fixed to this value based on speciation calculations.

The collection of high quality EXAFS data allowed assignment of the subtle features in the EXAFS spectra to the corresponding ligands, as well as the quantitative modeling described above. The structural parameters of the Cd–O, Cd–S, Cd–C and Cd–P contributions (paths) used in fitting the Cd sulfide, Cd-acetate and Cd-phosphate standards are the same as listed in Table 3 of Mishra et al., 2009. The presence of these contributions in the spectrum of an unknown sample can be taken as indicative of sulfhydryl-, carboxyl-, and phosphoryl- binding environments, respectively. Our approach was to use these well-calibrated paths in the analysis of the spectra for the bacterial samples. A Cd–Cd contribution (path) obtained from the fit of the CdS spectrum was used to test for the presence of Cd precipitation in each sample.

3.5. Qualitative analysis of spectra from the bacterial samples

The magnitude and real part of the Fourier transform data for the *B. subtilis* samples at various Cd loadings are

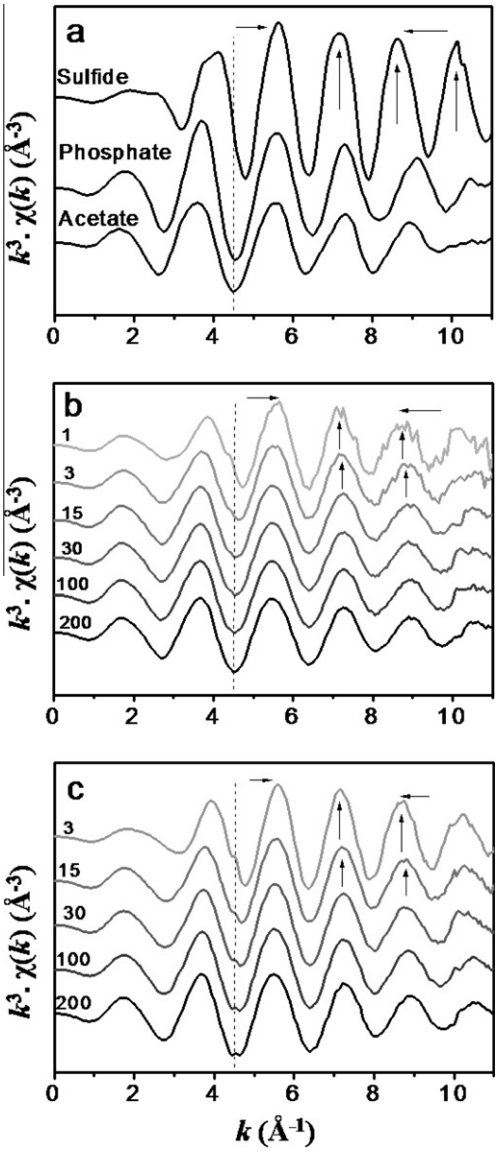

Fig. 3. (a) k^3 weighed $\chi(k)$ data for (a) the Cd standards, (b) *B. subtilis* isotherm, and (c) *S. oneidensis* isotherm data. Data range used for Fourier transform was 2.3–9.8 k (Å^{-1}).

shown in Fig. 4c and Fig. 4d, respectively. The data can be compared to the standards spectra that are depicted in Fig. 4a and b. An increase in the amplitude of the oscillation at 2.2 Å with decreasing Cd loading in the system can be clearly seen in Fig. 4d. Based on the analysis in the previous paragraph, this increase can be attributed to either increasing carboxyl or sulfhydryl binding to Cd. The choice between these two possibilities is based on the shift of the main peak position towards higher r values in Fig. 4c. As discussed above, this shift is characteristic of sulfhydryl binding, and suggests that in the two lowest concentration samples, 3.0 and 1.0 ppm, the adsorbed Cd is predominantly bound to sulfhydryl groups.

The magnitude and the real part of the Fourier transform data for the *S. oneidensis* samples are shown in Fig. 4e and Fig. 4f, respectively. A consistent increase in the amplitude oscillation and phase shift towards higher r value at about 2.2 Å occurs in the real part of the Fourier transform data (Fig. 4f) with decreasing Cd loading on the bacterial cell wall. By the same arguments as those applied to the *B. subtilis* spectra, we conclude that an increase in the relative amount of Cd atoms bound to sulfhydryl groups on the *S. oneidensis* cell wall occurs with decreasing Cd loading.

3.6. Quantitative EXAFS modeling

The six spectra from the samples taken along the *B. subtilis* isotherm were first fit independently, using the Cd–O, Cd–S, Cd–C and Cd–P paths that were used to model the Cd standards (Table 2). The numerical results from these fits are not shown because the final model, based on simultaneous fitting of data from all six Cd concentrations, yielded identical results but with smaller uncertainties. Below we discuss the individual fits separately only to show that the observed binding behavior with Cd concentration is not the result of the global fitting constraint.

We attempted to model the 200 ppm Cd *B. subtilis* spectrum with a single binding site and found that Cd-phosphoryl binding yields the best fit to the data. However, the addition of a Cd-carboxyl binding site to the Cd-phosphoryl model significantly improves the fit. There is no evidence for Cd-sulfhydryl binding in the 200 ppm Cd spectrum. Best-fit values of the path parameters (σ^2 and ΔR) for this sample were the same (within uncertainties) as those obtained for the Cd standards reported above. Modeling of the 100 ppm Cd *B. subtilis* spectrum yields results similar to those from the 200 ppm Cd spectrum, with phosphoryl and carboxyl binding able to yield an excellent fit to the data and with no evidence for Cd-sulfhydryl binding. Conversely, modeling of the individual spectra for the 30, 15, 3 and 1 ppm Cd samples requires an additional Cd-sulfhydryl binding site, and indicates an increase in the sulfhydryl coordination numbers with decreasing Cd concentration. While the carboxyl contribution to Cd binding remains constant (within error) over this concentration range, the phosphoryl contribution remains constant (within error) up to 15 ppm, decreases for 3 ppm, and was not required at all in order to successfully model the 1 ppm data. A steep increase in the sulfhydryl coordination number was found at 1 ppm, indicating the predominance of Cd-sulfhydryl binding under these conditions.

The Cd-sulfhydryl binding that we observed in the 30 ppm *B. subtilis* experiment, although only a small portion of the bound Cd budget, is in contrast with the findings of Boyanov et al. (2003) and Mishra et al. (2007) who did not report any sulfhydryl binding for the same bacterial species at similar Cd concentrations and pH values. However, the S coordination number that we report here for these conditions (0.08 ± 0.04) is extremely small, and could easily be masked by carboxyl and phosphoryl functional groups with small changes in experimental conditions.

Although independent modeling of the six *B. subtilis* samples provides an approximation of the contributions of Cd-carboxyl, -phosphoryl and -sulfhydryl binding in each spectrum, the average binding environment is complex

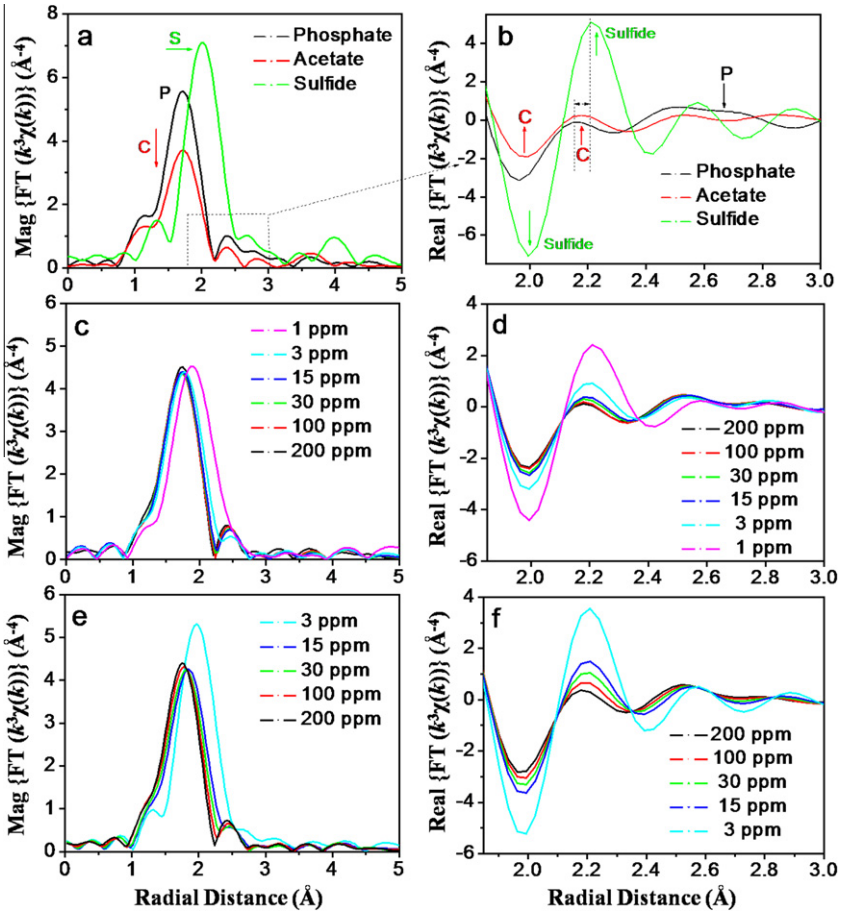

Fig. 4. (a) Fourier Transform magnitude of the Cd Standard data, (b) real part of the Fourier transform data of the Cd standard data, (c) Fourier Transform magnitude of the *B. subtilis* isotherm data, (d) real part of the Fourier Transform data of the *B. subtilis* isotherm, (e) Fourier Transform magnitude of the *S. oneidensis* isotherm data, and (f) real part of the Fourier Transform data of the *S. oneidensis* isotherm.

in nature and there are overlapping contributions of relatively small amplitude in the spectra. Correlations within each individual fit between coordination numbers and sigma-square values, as well as between ΔE_0 (energy shift) and bond distances, can mask trends in the structural parameters in the series of samples. To deal with the problem, all six spectra were fit simultaneously, each at three *k*-weights, resulting in a simultaneous fit of eighteen datasets. The energy shift, ΔE_o, the radial distance (R) and the distance variation (σ^2-value) to each ligand were refined, but were constrained to be the same in all samples. This approach carries in it the implicit assumption of identical molecular binding geometry to the corresponding ligands in all samples, and attributes the variation in amplitude to variations in the relative coordination numbers. In other words, it is assumed that the Cd–ligand distance and variation in average radial distance (σ^2-values) are the same whether Cd is bound to that ligand alone or is in a mixed environment of Cd-carboxyl, Cd-phosphoryl and/or Cd-sulfhydryl binding. This simultaneous fitting approach yields best-fit values of the path parameters (σ^2 and ΔR) for all paths that are the same (within uncertainties) as those obtained for the Cd standards (Table 2). These variables were therefore fixed to be equal to the values obtained for them from the Cd standards. The increased number of independent data points for the fit and the reduced number of variables resulted in smaller correlations between the fitting parameters, allowing their determination with smaller uncertainties and revealing the trends in average binding environment with changes in Cd loading.

Further confidence in the fitting approach adopted in this study was gained by a simple test to determine the robustness of the model. The variables (distances, and Debye–Waller factors) which have been fixed in this fitting approach to the values obtained by standard compounds were set to the upper and lower limits of their uncertainties and the fits were performed again (Table 2). This results in less than a 15% change in the final coordination numbers of the corresponding ligands reported in Table 3a. Although a rigorous qualitative modeling of the data has been attempted, and a robust fitting of the EXAFS spectra has been achieved, the determination of the absolute number of ligands bound to a metal in a complex natural system is difficult. However, the technique is much more precise in determining relative changes in the coordination environment of the metal, so the observed changes in the coordination numbers that we report in Table 3 are significant and real.

Table 3
EXAFS fitting parameters for (a) *B. subtilis* and (b) *S. oneidensis* samples.

[Cd] (in ppm)	1.0	3.0	15	30	100	200
(a) *Bacillus subtilis*						
Paths						
No	1.95 ± 0.16	3.93 ± 0.28	4.67 ± 0.16	4.78 ± 0.12	4.98 ± 0.16	4.93 ± 0.14
Nc	1.22 ± 0.52	1.23 ± 0.62	0.97 ± 0.48	0.89 ± 0.46	0.99 ± 0.60	0.98 ± 0.48
Ns	2.87 ± 0.14	0.98 ± 0.22	0.17 ± 0.14	0.08 ± 0.04		
Np		0.48 ± 0.24	0.82 ± 0.36	0.82 ± 0.32	1.12 ± 0.40	1.03 ± 0.40
Ro = 2.28 Å, $\sigma_o^2 = 0.009$ Å^{-2} Rc = 2.70 Å, $\sigma_c^2 = 0.012$ Å^{-2} Rs = 2.53 Å, $\sigma_s^2 = 0.009$ Å^{-2} Rp = 3.41 Å, $\sigma_p^2 = 0.015$ Å^{-2} $\Delta E_0 = -2.2 \pm 0.8$ eV						
(b) Shewanella oneidensis						
Paths						
No			3.18 ± 0.28	3.72 ± 0.22	4.28 ± 0.20	4.98 ± 0.14
Nc			1.17 ± 0.42	1.30 ± 0.56	1.46 ± 0.60	1.40 ± 0.54
Ns		4.10 ± 0.65	1.42 ± 0.14	0.90 ± 0.16	0.45 ± 0.16	
Np			0.35 ± 0.26	0.58 ± 0.30	0.83 ± 0.30	0.95 ± 0.34
Ro = 2.28 Å, $\sigma_o^2 = 0.009$ Å^{-2} Rc = 2.70 Å, $\sigma_c^2 = 0.012$ Å^{-2} Rs = 2.53 Å, $\sigma_s^2 = 0.009$ Å^{-2} Rp = 3.41 Å, $\sigma_p^2 = 0.015$ Å^{-2} $\Delta E_0 = -1.4 \pm 0.6$ eV						

The number of variables used to fit the EXAFS data in this study is less than one-third the number of independent data points in the data as obtained using Nyquist's theorem (Nyquist, 1928). Hence, the goodness-of-fit of the model to the data is not the result of excessive flexibility in the model and each refined parameter represents meaningful information about the binding environments.

Final fitting parameters for the *B. subtilis* system are tabulated in Table 3a, and the magnitude and real part of the Fourier transform of the data and fits are shown in Fig. 5a and b, respectively. Table 3a shows that the number of oxygen atoms bound to each Cd atom consistently decreases with decreasing Cd concentration from 4.93 ± 0.14 for the 200 ppm sample to 1.95 ± 0.16 for the 1.0 ppm sample. This is concurrent with an increase in the average number of sulfur atoms bound to each Cd atom from 0.8 ± 0.04 for 30 ppm to 2.87 ± 0.14 for the 1.0 ppm *B. subtilis* sample. The two highest Cd loading samples (200 and 100 ppm Cd) do not exhibit any sulfhydryl contribution to the Cd binding. The coordination numbers of the carboxyl group ($\sim 1.0 \pm 0.5$) remain the same within the uncertainty of the measurement over the entire concentration range measured. The coordination number of the phosphoryl group remains the same ($\sim 1.0 \pm 0.3$) within the uncertainty of the measurement for the 200, 100, 30 and 15 ppm Cd samples, but decreases to 0.48 ± 0.24 for the 3.0 ppm sample. The 1.0 ppm *B. subtilis* data do not require the inclusion of Cd-phosphoryl binding to account for the experimental spectra.

We used a similar approach to model the *S. oneidensis* data as we did for the *B. subtilis* data. That is, we first attempted to model each spectrum individually with as few site types as possible. We then compared these results with simultaneous fits of all of the spectra together. In general, we observed similar Cd binding environments and trends in the *S. oneidensis* samples as we did for the *B. subtilis* samples. Modeling of the 200 ppm Cd *S. oneidensis* spectrum with a single binding site provided the best fit with Cd-phosphoryl binding. However, as was the case for the 200 ppm Cd *B. subtilis* sample, the addition of Cd-carboxyl binding to the Cd-phosphoryl model significantly improved the fit. Best-fit values of the parameters (σ^2 and ΔR) for this sample are the same (within uncertainties) as those obtained for the Cd standards reported above. Modeling of the individual spectra for the 100, 30, and 15 ppm Cd samples shows an increase in the sulfhydryl coordination numbers with decreasing Cd concentration. While the carboxyl contribution to Cd binding remains constant (within error) over this concentration range, the phosphoryl contribution decreases with decreasing Cd concentration in the samples. A steep increase in sulfhydryl coordination number to 4.10 ± 0.65 occurs for the 3 ppm Cd sample, where carboxyl and phosphoryl contributions to Cd binding are not required to fit the data. This spectrum was fit solely with a Cd–S path, indicating the complete dominance of Cd-sulfhydryl binding under these conditions.

Final fitting parameters for the *S. oneidensis* system, using the same simultaneous fitting approach as we applied to the *B. subtilis* spectra, are listed in Table 3b, and the magnitude and real part of the Fourier transform of the measured spectra and the model fits are shown in Fig. 5c and d, respectively. Table 3b shows that the number of oxygen atoms bound to each Cd atom consistently decreases with decreasing Cd concentration from 4.98 ± 0.14 for the 200 ppm sample to 3.18 ± 0.28 for the 15 ppm sample. This is concurrent with an increase in the average number of S

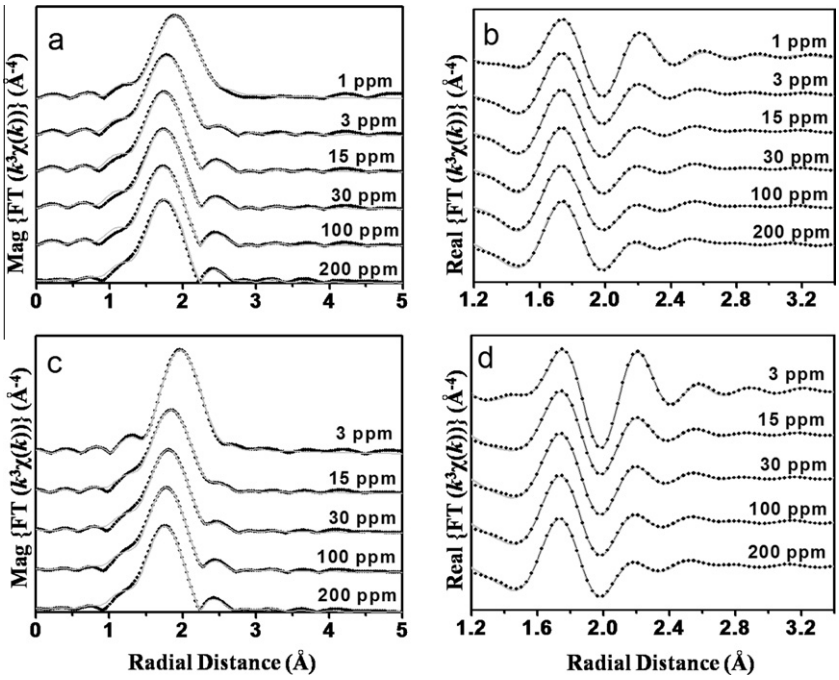

Fig. 5. Fourier Transform (a) magnitude and (b) real part of the EXAFS data and fits for the *B. subtilis* isotherm, and Fourier transform (c) magnitude and (d) real part of the EXAFS data and fits for the *S. oneidensis* isotherm.

atoms bound to each Cd atom from 0.45 ± 0.16 for the 100 ppm Cd sample to 1.42 ± 0.14 for the 15.0 ppm Cd-*S. oneidensis* sample. The highest Cd loading sample (200 Cd) does not exhibit any Cd-sulfhydryl contribution. The coordination numbers of the carboxyl group remain the same (1.30 ± 0.15) as a function of Cd loading within the uncertainty of the measurement. The coordination number of the phosphoryl group decreases from 0.95 ± 0.34 for the 200 ppm Cd sample to 0.35 ± 0.26 for the 15 ppm Cd-*S. oneidensis* sample. The 3 ppm Cd-*S. oneidensis* data were modeled with Cd-sulfhydryl binding only. Carboxyl and phosphoryl contributions to the Cd binding were not required for modeling the 3 ppm Cd data.

3.7. Discussion of Cd adsorption on bacterial cell walls as a function of Cd loading

The EXAFS fitting results are consistent with the modeling of the bulk adsorption data, and indicate that *B. subtilis* and the *S. oneidensis* cells exhibit broadly similar binding mechanisms for Cd as a function of metal loading under the conditions of this study. Phosphoryl and carboxyl binding are primarily responsible for Cd binding to *B. subtilis* cells at higher and intermediate Cd loading conditions (200, 100, 30 and 15). Carboxyl and sulfhydryl binding become much more important at 3 ppm and sulfhydryl sites become the most important binding sites at 1 ppm Cd loading for *B. subtilis*. On the other hand, phosphoryl binding dominates Cd binding to *S. oneidensis* cells under high Cd loading conditions (the 200 and 100 ppm Cd samples). The importance of carboxyl functional groups is highest at intermediate Cd loading conditions (the 30 and 15 ppm Cd samples) for *S. oneidensis*, due to the decreasing importance of the phosphoryl group. Sulfhydryl sites completely dominate the Cd binding for the *S. oneidensis* samples with the lowest Cd loading (3 ppm Cd). Sulfhydryl binding likely does not disappear with increasing Cd loading onto the bacterial cell wall. Rather, carboxyl and phosphoryl binding dominate the bound Cd budget under these conditions, swamping the signal of the relatively low abundance Cd-sulfhydryl sites. The EXAFS fitting parameters indicate that more than one site is involved simultaneously in Cd binding under most of the conditions studied, and except for the lowest Cd concentrations studied, the dominant adsorption stoichiometry for each site type is a 1:1 Cd:Site ratio. These results are consistent with the surface complexation modeling of the bulk Cd adsorption data, which also indicates an average Cd:Site stoichiometry of 1:1 and 1:2 at the high and low Cd concentration ranges of this study. The increase in average coordination number under the lowest Cd loading conditions is evident from the steepening of the Cd adsorption isotherms (Fig. 2a and b) under these conditions. In addition, if we determine the average adsorption stoichiometry that is consistent with only the data points with the lowest three Cd concentrations for each bacterial species, then we obtain best-fitting Cd:Site stoichiometries of 1:3 and 1:4 for the *B. subtilis* and the *S. oneidensis* data, respectively. These results are consistent with the increase in S coordination number to 2.87 ± 0.14 and 4.10 ± 0.65 for the lowest Cd concentrations studied for *B. subtilis* and *S. oneidensis*.

The lowest concentration *S. oneidensis* sample exhibits sulfhydryl binding only, and therefore can be used to estimate the concentration of sulfhydryl sites on the bacterial cell wall. Cd forms stable tetrahedral bonds with S, so our observed coordination number of 4.10 ± 0.65 for S is consistent with the absence of any carboxyl and/or phosphoryl binding of Cd in this sample. It would, therefore,

be reasonable to assume that for the 3 ppm Cd *S. oneidensis* sample, the concentration of sulfhydryl functional groups on the cell wall can be approximated as four times the concentration of adsorbed Cd atoms. This approximation is likely an underestimation, as not all sulfhydryl sites on the cell wall are involved in Cd binding under these conditions. However, these are the first estimates of the sulfhydryl site concentration and are valuable as preliminary constraints at least. Under these conditions, the concentration of adsorbed Cd is 2.2×10^{-6} moles of Cd per gram (wet mass) of bacteria, yielding an estimate of the sulfhydryl site concentration of 8.8×10^{-6} moles of sites per gram (wet mass) of bacteria. This site concentration represents only approximately 2% of the total number of sites on the cell wall, as determined by the potentiometric titrations.

The observation and characterization of the low abundance, high-affinity sulfhydryl sites in this study was made possible by using very low metal-to-surface loading conditions. This avoided masking of the sulfhydryl spectral signal by larger signals from the more abundant, lower-affinity sites that become occupied under higher metal loading conditions. A possible reason why purely sulfhydryl bonding has not been observed in previous spectroscopy studies was the use of high metal loadings in order to obtain good signal-to-noise ratio during data collection. We were able to collect high quality spectra from low concentration samples by utilizing a high-flux undulator beamline and a Stern–Heald fluorescence detector (Stern and Heald, 1983). The more intuitive approach of using a 13-element energy-dispersive Ge detector provided inferior data quality above $k \sim 8$ Å^{-1}. We explain this by the fact that our system is composed predominantly of low-Z elements, resulting in a low fluorescence background. Therefore, the advantage of removing the small background using energy-dispersive detectors is outweighed by the limited count rate compared to ionization chambers. In addition, by optimizing the gasses, voltages, and the sensitivity regimes of the incident and fluorescence ionization detectors we were able to achieve a better linear response between the *Io* and *If* detectors. This resulted in low-noise data from samples as dilute as 1 ppm Cd in the original solution phase.

4. CONCLUSIONS

This study highlights the strengths and limitations of both bulk adsorption and EXAFS measurements of metal–bacterial complexation. Bulk metal adsorption measurements conducted as a function of metal loading provide constraints on the average adsorption reaction stoichiometry, and enable quantification of the stability constants for the important metal-bacterial complexes. However, these measurements do not provide for direct identification of the important site or sites involved in metal binding. Conversely, EXAFS measurements can rigorously identify the important adsorption sites, but are less precise for determining reaction stoichiometry and stability constant values.

We use these complementary techniques to elucidate the nature and extent of Cd adsorption onto typical Gram-positive and Gram-negative bacterial cell walls. The bulk Cd adsorption measurements indicate that adsorption can be reasonably explained by a 1:1 metal:site reaction stoichiometry over the range of metal loading conditions studied here. The EXAFS results are consistent with the bulk adsorption measurements, indicating monodentate binding of Cd onto both the carboxyl and the phosphoryl sites. The only conditions where multi-dentate binding was observed in the EXAFS data were for the lowest Cd loading samples for both species (1 ppm for *B. subtilis* and 3 ppm for *S. oneidensis)*, where the coordination number for the sulfhydryl binding site becomes significantly greater than one.

The EXAFS measurements, collected over two orders of magnitude of Cd:site loading conditions, indicate similar binding environments for the two bacterial species studied. In addition, the EXAFS modeling indicates that three different sites are responsible for Cd binding to these two bacterial cell walls. Fig. 6 depicts the general predominance regions for the three different types of sites as a function of Cd loading for the *S. oneidensis* samples, and a similar picture would apply to the *B. subtilis* samples as well. Phosphoryl and carboxyl binding play important roles at high (100–200 ppm) and mid (15–30 ppm) Cd loadings, respectively, for the *S. oneidensis* samples. For the *B. subtilis* samples, phosphoryl and carboxyl sites exhibit overlapping and equal contributions for the samples with Cd concentrations of 15 ppm and higher. Carboxyl binding becomes more important than phosphoryl binding at 3 ppm Cd loading for *B. subtilis* samples. However, at the lowest Cd loadings for both of the species studied here, sulfhydryl surface complexes dominate the adsorbed Cd budgets. Because the sulfhydryl binding sites out-compete other deprotonated sites for Cd at low Cd concentrations, these sites must have a higher binding affinity for Cd than the other sites that are deprotonated at pH 5.9. However, the EXAFS data in this study do not constrain the location or identity of the sulfhydryl groups that bind Cd onto the biomass. The sulfhydryl sites may be a component of cell wall-bound metal regulator proteins, or they may represent a component of a toxicity response mechanism located on the cell walls, initiated by the non-metabolizing cells with the small amount of stored energy that remains after washing. Our EXAFS

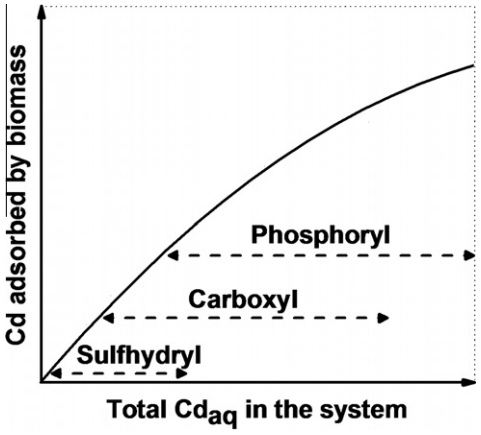

Fig. 6. A schematic representation of the regions of predominance of the three different Cd binding environments as a function of Cd loading onto biomass as determined by EXAFS.

analysis indicates that the sulfhydryl sites are limited in abundance relative to other cell wall site types, their binding stoichiometries with Cd are much higher than those found for the other functional groups, and these multi-dentate bonds bind Cd tightly. However, a precise determination of the location and more general molecular structure of the sulfhydryl sites require additional experimental and analytical constraints.

Because of the overlapping ranges of the phosphoryl, carboxyl, and sulfhydryl binding, we could not explicitly determine the stability constant for each Cd–bacterial surface complex for each species studied here. However, because a single stability constant yielded an excellent fit to the bulk Cd adsorption data over a wide range of Cd loading conditions, the value of this stability constant represents the average of the individual stability constants of the Cd-sulfhydryl, the Cd-carboxyl, and the Cd-phosphoryl bacterial surface complexes. Potentiometric titrations and Cd adsorption measurements that explicitly probe conditions under which these sites each dominate are needed in order to explicitly determine the speciation and thermodynamic stability of each complex.

The EXAFS results presented in this study demonstrate the following: (1) there is a broad similarity between the Cd binding environments of these two species over a wide range of Cd concentrations at circumneutral pH conditions, and (2) Cd-sulfhydryl binding dominates the adsorbed Cd budget under low Cd loading conditions. The similarity in the extent of bulk Cd adsorption of these two bacterial species over a wide range of Cd loadings complements the recent finding that diverse bacterial consortia exhibit broadly similar binding environments over a wide pH range at a fixed Cd loading (Mishra et al., 2009; Johnson et al., 2007; Borrok et al., 2004b). Metal-sulfhydryl binding likely occurs under the higher Cd loading conditions studied here, but its presence is masked to EXAFS probing by the relatively high-abundance of carboxyl and phosphoryl binding sites when metal:-site molal concentration ratios are high. However, our data indicate the important role of these sites in Cd binding to both Gram-positive and Gram-negative bacterial cells under the circumneutral pH conditions of many natural systems. Since Cd represents typical trace metal binding (e.g., Fein, 2000), sulfhydryl binding is likely to control metal binding under low loading conditions for a wide range of metals of environmental and geologic interest. Our finding that sulfhydryl is the dominant binding ligand at lower Cd loadings suggests that these sites may also dominate metal binding by bacteria in realistic geologic settings where metals are typically present in trace concentrations.

ACKNOWLEDGMENTS

Research funding was provided by a National Science Foundation through an Environmental Molecular Science Institute Grant to the University of Notre Dame (EAR02-21966), and from a Bayer Corporation Predoctoral Fellowship. S.D.K. and K.M.K. were supported by the US Department of Energy office of Science Biological and Environmental Research Division Environmental Remediation Science Program. MRCAT is supported by the US Department of Energy under contract DE-FG02-94-ER-45525 and the member institutions. Use of the Advanced Photon Source was supported by the US Department of Energy under contract W-31-109-Eng-38. Some analyses were conducted using instruments in the Center for Environmental Science and Technology at University of Notre Dame. Help in sample preparation from Jennifer Szymanowski, and beamline setup help from Tomohiro Shibata and Soma Chattopadhyay of MRCAT are greatly appreciated. Two anonymous journal reviewers and Associate Editor Michael Machesky made helpful suggestions and significantly improved the clarity of this paper.

REFERENCES

Ankudinov A. L., Ravel B., Rehr J. J. and Conradson S. D. (1998) Real-space multiple-scattering calculation and interpretation of X-ray-absorption near-edge structure. *Phys. Rev. B* **58**, 7565–7576.

Beveridge T. J. and Murray R. G. E. (1980) Sites of metal deposition in the cell wall of *Bacillus subtilis*. *J. Bacteriol.* **141**, 876–887.

Borrok D., Fein J. B. and Kulpa C. F. (2004a) Proton and Cd adsorption onto natural bacterial consortia: testing universal adsorption behavior. *Geochim. Cosmochim. Acta* **68**, 3231–3238.

Borrok D. M., Fein J. B. and Kulpa C. F. (2004b) Cd and proton adsorption onto bacterial consortia grown from industrial wastes and contaminated geologic settings. *Environ. Sci. Technol.* **38**, 5656–5664.

Borrok D., Fein J. B. and Turner B. F. (2005) A universal surface complexation framework for modeling proton binding onto bacterial surfaces in geologic settings. *Am. J. Sci.* **305**, 826–853.

Boyanov M. I., Kelly S. D., Kemner K. M., Bunker B. A., Fein J. B. and Fowle D. A. (2003) Adsorption of cadmium to *Bacillus subtilis* bacterial cell walls: a pH-dependent X-ray absorption fine structure spectroscopy study. *Geochim. Cosmochim. Acta* **67**, 3299–3311.

Burnett P. G. G., Daughney C. J. and Peak D. (2006) Cd adsorption onto *Anoxybacillus flavithermus*: Surface complexation modeling and spectroscopic investigations. *Geochim. Cosmochim. Acta* **70**, 5253–5269.

Claessens J., Behrends T. and Van Cappellen P. (2004) What do acid–base titrations of live bacteria tell us? A preliminary assessment. *Aqua Sci* **66**, 19–26.

Caminiti R. (1982) Nickel and cadmium phosphates in aqueous-solution – cation anion complex-formation and phosphate–H_2O interactions. *J. Chem. Phys.* **77**, 5682–5686.

Caminiti R., Cucca P., Monduzzi M., Saba G. and Crisponi G. (1984) Divalent metal–acetate complexes in concentrated aqueous-solutions – an X-ray-diffraction and NMR-spectroscopy study. *J. Chem. Phys.* **81**, 543–551.

Cox J. S., Smith D. S., Warren L. A. and Ferris F. G. (1999) Characterizing heterogeneous bacterial surface functional groups using discrete affinity spectra for proton binding. *Environ. Sci. Technol.* **33**, 4515–4521.

Daughney C. J., Fein J. B. and Yee N. (1998) A comparison of the thermodynamics of metal adsorption onto two common bacteria. *Chem. Geol.* **144**, 161–176.

Daughney C. J., Sicilliano S. D., Rencz A. N., Lean D. and Fortin D. (2002) Hg(II) adsorption by bacteria: a surface complexation model and its application to shallow acidic lakes and wetlands in Kejimkujik National Park, Nova Scotia, Canada. *Environ. Sci. Technol.* **36**, 1546–1553.

Fein J. B. (2000) Quantifying the effects of bacteria on adsorption reactions in water–rock systems. *Chem. Geol.* **169**, 265–280.

Fein J. B., Daughney C. J., Yee N. and Davis T. A. (1997) A chemical equilibrium model for metal adsorption onto bacterial surfaces. *Geochim. Cosmochim. Acta* **61**, 3319–3328.

Fein J. B., Boily J. F., Yee N., Gorman-Lewis D. and Turner B. F. (2005) Potentiometric titration of *Bacillus subtilis* cells to low pH and a comparison of modeling approaches. *Geochim. Cosmochim. Acta* **69**, 1123–1132.

Fowle D. A. and Fein J. B. (2000) Experimental measurements of the reversibility of metal–bacteria adsorption reactions. *Chem. Geol.* **168**, 27–36.

Guiné V., Spadini L., Sarret G., Muris M., Delolme C., Gaudet J. P. and Martins J. M. F. (2006) Zinc sorption to three Gram-negative bacteria: combined titration, modeling, and EXAFS study. *Environ. Sci. Technol.* **40**, 1806–1813.

Harden V. and Harris J. O. (1952) The isoelectric point of bacterial cells. *J. Bacteriol.* **65**, 198–202.

Haas J. R., Dichristina T. J. and Wade, Jr., R. (2001) Thermodynamic of U(VI) sorption onto *Shewanella putrefaciens*. *Chem. Geol.* **180**, 33–54.

Hennig C., Panak P. J., Reich T., Rossberg A., Raff J., Selenska-Pobell S., Matz W., Bucher J. J., Bernhard G. and Nitsche H. (2001) EXAFS investigation of uranium(VI) complexes formed at Bacillus cereus *and Bacillus sphaericus* surfaces. *Radiochim. Acta* **89**, 625–631.

Kelly S. D., Kemner K. M., Fein J. B., Fowle D. A., Boyanov M. I., Bunker B. A. and Yee N. (2002) X-ray absorption fine structure determination of pH-dependent U-bacterial cell wall interactions. *Geochim. Cosmochim. Acta* **66**, 3855–3871.

Kemner K. M., Kropf A. J. and Bunker B. A. (1994) A low-temperature total electron yield detector for X-ray absorption fine structure spectra. *Rev. Sci. Instrum.* **65**, 3667–3669.

Kulczycki E., Fowle D. A., Fortin D. and Ferris F. G. (2005) Sorption of cadmium and lead by bacteria–ferrihydrite composites. *Geomicrobiol. J.* **22**, 299–310.

Ledin M., Krantz-Rulcker C. and Allard B. (1996) Zn, Cd and Hg accumulation by microorganisms, organic and inorganic soil components in multi-compartment systems. *Soil Biol. Biochem.* **28**, 791–799.

Ledin M., Krantz-Rulcker C. and Allard B. (1999) Microorganisms as metal sorbents: comparison with other soil constituents in multi-compartment systems. *Soil Biol. Biochem.* **31**, 1639–1648.

Ledin M. (2000) Accumulation of metals by microorganisms-processes and importance for soil systems. *Earth-Sci. Rev.* **51**, 1–31.

Leone L., Ferri D., Manfredi C., Persson P., Shchukarev A., Sjoberg S. and Loring J. (2007) Modeling the acid–base properties of bacterial surfaces: a combined spectroscopic and potentiometric study of the Gram-positive bacterium *Bacillus subtilis*. *Environ. Sci. Technol.* **41**, 6465–6471.

Martinez R. E., Smith D. S., Kulczycki E. and Ferris F. G. (2002) Determination of intrinsic bacterial surface acidity constants using a donnan shell model and a continuous pK(a) distribution method. *J. Colloid Interface Sci.* **253**, 130–139.

Mishra B., Fein J. B., Boyanov M. I., Kelly S. D., Kemner K. M. and Bunker B. A. (2007) Comparison of Cd binding mechanisms by Gram-positive, Gram-negative and consortia of bacteria using XAFS. *AIP Conf. Proc.* **882**, 343–345.

Mishra B., Boyanov M. I., Bunker B. A., Kelly S. D., Kemner K. M., Nerenberg R., Read-Daily B. L. and Fein J. B. (2009) An X-ray absorption spectroscopy study of cd binding onto bacterial consortia. *Geochim. Cosmochim. Acta* **73**, 4311–4325.

Nealson K. H. and Myers C. R. (1992) Microbial reduction of manganese and iron: new approaches to carbon cycling. *Appl. Environ. Microbiol.* **58**, 439–443.

Newville M. (2001) IFEFFIT: interactive XAFS analysis and FEFF fitting. *J. Sync. Rad.* **8**, 322–324.

Newville M., Ravel B., Haskel D., Rehr J. J., Stern E. A. and Yacoby Y. (1995) Analysis of multiple-scattering Xafs data using theoretical standards. *Physica B* **209**, 154–156.

Newville M., Livins P., Yacoby Y., Rehr J. J. and Stern E. A. (1993) Near-edge X-ray-absorption fine-structure of Pb – a comparison of theory and experiment. *Phys. Rev. B* **47**, 14126–14131.

Ngwenya B. T., Sutherland I. W. and Kennedy L. (2003) Comparison of the acid–base behaviour and metal adsorption characteristics of a Gram-negative bacterium with other strains. *Appl. Geochem.* **18**, 527–538.

Ngwenya B. T. (2007) Enhanced adsorption of zinc is associated with aging and lysis of bacterial cells in batch incubations. *Chemosphere* **67**, 1982–1992.

Nyquist H. (1928) Certain topics in telegraph transmission theory. *Trans. AIEE* **47**, 617–644.

Ohnuki T., Yoshida T., Ozaki T., Kozai N., sakamoto F., Nankawa T., Suzuki Y. and Francis A. J. (2007) Chemical Speciation and association of plutonium with bacteria, kaolinite clay, and their mixture. *Environ. Sci. Technol.* **41**, 3134–3139.

Panak P. J., Booth C. H., Caulder D. L., Bucher J. J., Shuh D. K. and Nitsche H. (2002) X-ray absorption fine structure spectroscopy of plutonium complexes with *Bacillus sphaericus*. *Radiochim. Acta* **90**, 315–321.

Pokrovsky O. S., Martinez R. E., Golubev S. V., Kompantseva E. I. and Shirokova L. S. (2008a) Adsorption of metals and protons on *Gloeocapsa* sp. cyanobacteria: a surface speciation approach. *Appl. Geochem.* **23**, 2574–2588.

Pokrovsky O. S., Pokrovsky G. S. and Feurtet-Mazel A. (2008b) A structural study of Cd interaction with aquatic microorganisms. *Environ. Sci. Technol.* **42**, 5527–5533.

Plette A. C. C., Vanriemsdijk W. H., Benedetti M. F. and Vanderwal A. (1995) pH dependent charging behavior of isolated cell-walls of a Gram-positive soil bacterium. *J. Colloid Interface Sci.* **173**, 354–363.

Ravel B. (2001) ATOMS: crystallography for the X-ray absorption spectroscopist. *J. Sync. Rad.* **8**, 314–316.

Ravel B. and Newville M. (2005) Athena, artemis, hephaestus: data analysis for X-ray absorption spectroscopy using IFEFFIT. *J. Sync. Rad.* **12**, 537–541.

Sarret G., Manceau A., Spadini L., Roux J. C., Hazemann J. L., Soldo Y., Eybert-Berard L. and Menthonnex J. J. (1998) Structural determination of Zn and Pb binding sites in *Penicillium chrysogenum* cell walls by EXAFS spectroscopy. *Environ. Sci. Technol.* **32**, 1648–1655.

Segre C. U., Leyarovska N. E., Chapman L. D., Lavender W. M., Plag P. W., King A. S., Kropf A. J., Bunker B. A., Kemner K. M., Dutta P., Duran R. S. and Kaduk J. (2000) The MRCAT insertion device beamline at the advanced photon source. *Sync. Rad. Instrum: 11th US Conf.* **CP521**, 419–422.

Small T. D., Warren L. A., Roden E. E. and Ferris F. G. (1999) Sorption of strontium by bacteria, Fe(III) oxide, and bacteria–Fe(III) oxide composites. *Environ. Sci. Technol* **33**, 4465–4470.

Smith D. S. and Ferris F. G. (2003) Specific surface chemical interactions between hydrous ferric oxide and iron-reducing bacteria determined using pK_a spectra. *J. Colloid Interface Sci.* **266**, 60–67.

Sokolov I., Smith D. S., Henderson G. S., Gorby Y. A. and Ferris F. G. (2001) Cell surface electrochemical heterogeneity of the Fe(III)-reducing bacteria *Shewanella putrefaciens*. *Environ. Sci. Technol.* **35**, 341–347.

Sorenson J. (1982) Reduction of ferric iron in anaerobic, marine sediment, and interaction with reduction of nitrate and sulphate. *Appl. Environ. Microbiol.* **43**, 319–324.

Stern E. A. (1974) Theory of extended X-ray absorption fine structure. *Phys. Rev. B.* **10**, 3027–3037.

Stern E. A. and Heald S. M. (1983) Basic principles and applications of EXAFS. *Handbook Sync. Rad.* **10**, 995–1014.

Stern E. A., Newville M., Ravel B., Yacoby Y. and Haskel D. (1995) The Uwxafs analysis package – philosophy and details. *Physica B* **209**, 117–120.

Toner B., Manceau A., Marcus M. A., Millet D. B. and Sposito G. (2005) Zinc sorption by a bacterial biofilm. *Environ. Sci. Technol.* **39**, 8288–8294.

Venkateswaren K., Moser D. P., Dollhopf M. E., Lies D. P., Saffarini D. A., MacGregor B. J., Ringelberg D. B., White D. C., Nishijima M., Sano H., Burghardt J., Stackebrandt E. and Nealson K. H. (1999) Polyphasic taxonomy of the genus *Shewanella* and description of *Shewanella oneidensis* sp. nov. *Int. J. Sys. Bacteriol.* **49**, 705–724.

Wei J., Saxena A., Song B., Ward B. B., Beveridge T. J. and Myneni S. C. B. (2004) Elucidation of functional groups on Gram-positive and Gram-negative bacterial surfaces using infrared spectroscopy. *Langmuir* **20**, 11433–11442.

Westall, J. C. (1982) FITEQL, a computer program for determination for chemical equilibrium constants from experimental data. Version 2.0. Report 82-02 Dept. Chem., Oregon St. Univ., Corvallis, OR, USA.

Wightman P. G. and Fein J. B. (2005) Iron adsorption by *Bacillus subtilis* bacterial cell walls. *Chem. Geol.* **216**, 177–189.

Yee N. and Fein J. (2001) Cd adsorption onto bacterial surfaces: a universal adsorption edge? *Geochim. Cosmochim. Acta* **65**, 2037–2042.

Yee N. and Fein J. B. (2003) Quantifying metal adsorption onto bacteria mixtures: a test and application of the surface complexation model. *Geomicrobiol. J.* **20**, 43–60.

Yee N., Fowle D. A. and Ferris F. G. (2004) A donnan potential model for sorption onto *Bacillus subtilis*. *Geochim. Cosmochim. Acta* **68**, 3657–3664.

Associate editor: Michael L. Machesky